EFDA–JET–CP(12)06/22

T. Pütterich, R Dux, M.N.A. Beurskens, V. Bobkov, S. Brezinsek, J. Bucalossi, J.W. Coenen, I. Coffey, A. Czarnecka, C. Giroud, E. Joffrin, K.D. Lawson, M. Lehnen, E. de la Luna, J. Mailloux, S. Marsen, M.-L. Mayoral, A Meigs, R. Neu, F. Rimini, M. Sertoli, M. Stamp, G. van Rooij
and JET EFDA contributors

Tungsten Screening and Impurity Control in JET

Tungsten Screening and Impurity Control in JET

T. Pütterich[1], R Dux[1], M.N.A. Beurskens[2], V. Bobkov[1], S. Brezinsek[3], J. Bucalossi[4], J.W. Coenen[3], I. Coffey[5], A. Czarnecka[6], C. Giroud[2], E. Joffrin[4], K.D. Lawson[2], M. Lehnen[3], E. de la Luna[7], J. Mailloux[2], S. Marsen[8], M.-L. Mayoral[2], A Meigs[2], R. Neu[1], F. Rimini[2], M. Sertoli[1], M. Stamp[2], G. van Rooij[9] and JET EFDA contributors*

JET-EFDA, Culham Science Centre, OX14 3DB, Abingdon, UK

[1]Max-Planck-Institut f¨ur Plasmaphysik, EURATOM Association, 85748 Garching, Germany
[2]EURATOM-CCFE Fusion Association, Culham Science Centre, OX14 3DB, Abingdon, OXON, UK
[3]Institute of Energy- and Climate Research, Forschungszentrum J¨ulich, Association EURATOM-FZJ, Germany
[4]CEA, Association EURATOM-CEA, IRFM, Cadarache 13108 Saint Paul Lez Durance, France
[5]Queen's University Belfast, University Road, Belfast BT7 1NN, Northern Ireland, UK
[6]EURATOM Association, Institute Plasma Physics & Laser Microfus, PL-01497Warsaw, Poland
[7]EURATOM CIEMAT Association, Laboratorio Nacional de Fusión, Madrid, Spain
[8]Max-Planck-Institut für Plasmaphysik, EURATOM Association, D-17491 Greifswald, Germany
[9]DIFFER, Association EURATOM-FOM, 3430BE Nieuwegein, Netherlands
** See annex of F. Romanelli et al, "Overview of JET Results", (24th IAEA Fusion Energy Conference, San Diego, USA (2012)).*

Preprint of Paper to be submitted for publication in Proceedings of the
24th IAEA Fusion Energy Conference (FEC2012), San Diego, USA
8th October 2012 - 13th October 2012

ABSTRACT

The impact of tungsten on stability and confinement of plasma discharges is studied in JET featuring the ITER-like wall. AW-diagnostic combining the soft X-ray cameras and a VUV spectrometer was used to analyze the balance between heating and radiative cooling in the core plasma. In a typical example discharge featuring impurity accumulation, the core W radiation is quantified. It is strong enough to affect the Te-profiles. The flattening of the Te-profile is thought to cause a further reduction of turbulent transport including a turbulent outward pinch. In this situation the neoclassical inward pinch is provided with more weight, which leads to further accumulation of W. Smaller deuterium gas puff levels which lead to low ELM frequencies allow for a more efficient penetration of eroded W into the main plasma. For low gas puff conditions, also W-erosion and electron density peaking foster impurity accumulation which ought to be mitigated by a medium sized gas puff in the range of 1-2×1022 electrons/s.

1. INTRODUCTION

In a fusion reactor, a central tungsten (W) concentration of only 3×10^{-5} increases the minimum triple product for ignition nTE by 20% and at 1.9×10^{-4} the ignition condition can not be reached [1]. Tungsten is used as a plasma facing component in today's experiments, e.g. ASDEX Upgrade [2] and JET [3], and one objective is to quantify the mechanisms that determine the W-concentration in the plasma, when using W as a first wall material. While a stepwise transition at ASDEX Upgrade allowed to document the relative importance of various components for a full W device JET's ITER-like wall was implemented during one shut down allowing an easier comparison with the previous carbon plasma facing components (PFCs). The PFCs resemble the wall mix of ITER featuring W in the divertor and Beryllium (Be) in the main chamber. Now the most abundant impurity originating from the walls in JET is beryllium and the carbon concentrations have been reduced by factors of 10-20 which results in levels of 0.05% [4]. In JET, the Be dominates the low-Z impurity mix and thus the W erosion [5,6]. In ASDEX Upgrade, W has been observed to be well screened by the divertor plasma, see for example [7,8], and is thus thought to play also a minor role in the main plasma of JET and ITER. The W-screening in the divertor of JET is investigated and quantified in the present work.

Unexpectedly,Weventually affects the main plasma for the ITER-like wall experiments at JET. The properties of these effects are investigated and characterized. To this end details of a specific discharge featuring impurity accumulation are analyzed. This allows for understanding the processes that lead to and govern impurity accumulation, which is the biggest concern when dealing with W. At the same time a comprehensive database of pulses has been built which enables the testing of these findings. Due to space limitations the latter will be presented elsewhere.

2. QUANTITATIVE DIAGNOSIS OF THE W-DENSITY

Two approaches are chosen to provide a quantitative measure for the W-content in the core plasma.

In Fig.1 the lines of sight of two soft X-ray (SXR) cameras and a VUV spectrometer are depicted. The first approach makes use of the spectrometer which is set to 5nm where a strong spectral feature of the W-ions W^{27+} to W^{35+} is emitted (cf. [9]). This spectral feature, also called 'quasicontinuum', is emitted at electron temperatures between about 0.8-1.8keV. Its intensity is interpreted by taking the geometry, and electron density and temperature profiles into account and combining those with the atomic data of W as presented in [9]. In order to provide robust absolute numbers for the W-concentration a recalibration of the procedure is performed for radiation events that are known to be caused by W only. Such radiation events can be intentional laser ablations, but also natural events for which other radiators could be excluded by survey spectroscopy. For these events the total radiated power is connected to an absolute W-concentration via the cooling factor of W (cf. [1]), which is a robust number independently of the evaluation method used. The spectrometer provides W-concentrations that are valid only in a limited radial range, where the ambient Te allows the emission. Poloidal asymmetries, especially in-out asymmetries, might lead to an underestimation of the W-concentration. However, spectroscopy provides a direct method to determine the Wconcentration independently of other radiators in the plasma.

The second approach is using the SXR cameras to determine the W-concentrations. The large number of lines of sight allows determining a 2D radiation profile and poloidal asymmetries can easily be handled. However, it is not unambiguous what species in the plasma are responsible for the radiation in the soft X-ray range. Additionally, the atomic data that is necessary for the interpretation yield systematic uncertainties. As a result we needed to apply correction factors to come to a consistent picture with total radiated power and spectrometer measurements.

While the spectrometer data is not explained in the present work (for that cf. [9,10]), the SXR data interpretation is described in this paragraph. In a first approach, several discharges with a low content of W and other soft X-ray radiators have been analyzed. In these discharges the electron density and temperature measurements from high resolution Thomson scattering (HRTS) and LIDAR have been used to predict the local SXR emissivities due to Bremsstrahlung. The lines-of-sight integrals are then performed using their geometry and a magnetic equilibrium from EFIT. In order to simulate the resulting signal of the vertical and horizontal camera the corresponding beryllium filter thicknesses of 250 and 350 microns are taken into account, while for the response of the diodes themodel of [11] has been implemented. Unfortunately, a simple assumption of $Z_{eff} = 1$ already predicts higher signals than measured.

Thus, it is assumed that the absolute calibration of the SXR signals requires a correction factor of unknown origin. When using a realistic Z_{eff} -value (typically between 1 and 1.5, flat profile assumed), as derived from line-of-sightintegrated Bremsstrahlung measurements in the visible range, correction factors of 2.8 and 2.5 are derived for the vertical and horizontal camera, respectively. As a second step the Pulse No: 80891 has been analyzed which features W-concentrations between 5×10^{-5} to 2×10^{-4} and flat Wconcentration profiles, as measured by spectroscopy and bolometry. In Pulse No: 80891 only ICRH heating is used leading to low plasma rotation and the soft X-ray

radiation is observed to be poloidally symmetric. In order to derive absolute W-concentrations from the SXR camera signals the Bremsstrahlung contribution due to low-Z ions is subtracted and the excess radiation is attributed to W.

This excess radiation is then interpreted using the atomic data as derived in [9,1] while the Be filters and diode responses are taken into account. On top of line radiation and radiative recombination a rough model for dielectronic recombination is included. The model attributes to each dielectronic recombination process a photon with an average energy of half the ionization potential. When taking this dataset into account a discrepancy is found between the W-concentrations derived from the spectrometer (blue) and SXR cameras (grey) (cf. Fig.2). The discrepancy is larger for the phases with lower plasma temperature.

The presented error bars are obtained by propagating a 10%-uncertainty of the measured electron densities and temperatures. This 10%-level is thought to capture the typical differences between different electron density and temperature diagnostics. The discrepancy fits to the fact, that the description of the atomic data at the low energy cutoff of the Be-filter is most probably not correct. When considering the modeled spectra in [9], an energy cut off at about 0.5nm leaves only very small spectral lines of W-ions with charges larger than 38+ within the sensitivity window of the SXR cameras. Thus, unconsidered emissions from higher-n transitions or radiation from dielectronic recombination may change the emissions noticeably. An energy dependent correction factor has been used to adjust the atomic data. The original and adjusted data are presented in Fig.3. When using the adjusted dataset the derivedW-concentrations (black) in Fig.2 agree well with the spectrometer values and the W-concentration profiles are flatter, while with the original dataset they have been hollow. It should be noted that there are un4 certainties for the case that the Zeff -value exhibits strong radial variations as for the subtraction of the Bremsstrahlung background a radially constant Zeff is used. For the chosen discharge #80891 the measured signals in the core are much larger than the predicted Bremsstrahlung, such that the uncertainties attributed to Zeff are negligible. Thus, the correction factor determined here is used through-out the interpretation of the SXR camera signals.

3. EFFECTS OFWON DISCHARGE EVOLUTION

In the 2011/2012 campaigns effects of W on the main plasma have been observed that influence the stability of a plasma discharge especially for beam heated discharges. In Fig.4 time traces of selected parameters in such a discharge are presented.

The discharge with $I_p = 2.0$MA has been performed at a magnetic field of 2.1T yielding a $q_{95} = 3.3$. The ELM-frequency of the type-I ELMy H-mode was about 10-15Hz. From 9.0s on the deuterium gas puff is lowered to 5×10^{-21} m^{-3}. Up to 11.5s the diamagnetic energy (W_{dia}) does not considerably change, while the radiated power in the main chamber (P_{rad}) constantly increases. A steep increase of P_{rad} is observed after 11.5s affecting (W_{dia}) of the plasma. From 9.0s to 11.5s, the core electron temperature (T_e) as measured by electron cyclotron emission (ECE) keeps falling while the edge values stay constant (cf. Fig. 4(b)). During the same period the electron density

(n_e) (cf. Fig.4 (c)), as measured by HRTS, keeps rising in the plasma core and the edge values stay constant, which implies that the density starts peaking. Only after 11.5s the core T_e collapses drastically. These observations are also reflected in the evolution of the confinement H98-factor (cf. Fig.4(d)), which is 0.85 during the flattop and drops at the end of the flattop. As the lineaveraged $Z_{eff} \approx 1.2$ and does not change much during the radiation rise a medium to high-Z element must be the responsible for it. However, the W-concentration (c_W) as measured by the spectrometer stays constant through out. In order to estimate the radiated power due to W, the W-concentration, which is locally measured at a certain radial range, is assumed to apply for the full plasma volume - this estimate is depicted in Fig.4(a) and labeled 'est. W-rad'. The W-radiation seems to be negligible during all phases of the discharge and thus seems to indicate that W may not be responsible for the rise of the main chamber radiation. However, the spectrometer line of sight is vertical (cf. Fig.1) and may be missing parts of the W emissions because of poloidal asymmetries that arise from centrifugal forces. A further complication is that the W emissions seen by VUV spectrometer yield information from a limited radial region only. Indeed, the vertical SXR camera shows clear signs of poloidal asymmetries when looking at the line-of-sight-integrated raw signals. Thus, as described in section 2 a 2D deconvolution of the radiation attributed to W was performed, allowing for poloidal asymmetries which are consistent with the Wesson-formula [12]. The W-density on a flux surface is thus described by

$$n_W(r_{norm}, R) = n_{W,0}(r_{norm}) e^{\lambda(r_{norm})(R^2 - R_0^2(r_{norm}))},$$

where R is the large radius and $n_{W,0}(r_{norm})$ is the W-density on the flux surface labeled rnorm at the large radius $R_0(r_{norm})$. (r_{norm}) contains the dependence on the rotational frequency of the plasma. For the case that all plasma species have the same temperature it is given by:

$$\lambda(r_{norm}) = \left(1 - 0.5 Z_W \frac{m_D}{m_W}\right) \frac{m_W \omega^2}{2 T_W}$$

When the SXR analysis is applied to Pulse No: 81913 the strong asymmetries in measurements of the vertical SXR camera are translated into local poloidal asymmetries. The measured data is well described by the deconvolutions presented in Fig.5(a) and (b). The asymmetries show up most clearly just outside of the sawtooth inversion radius. If the radiation is purely caused by W, a rotation velocity of about 80km/s is required to explain the poloidal asymmetry. The measurements of charge-exchange recombination spectroscopy are consistent with that. As Ni is a candidate impurity for causing SXR radiation, the Ni levels have been checked by additional spectroscopic measurements (cf. [13]) and a major contribution of Ni can be excluded. Additionally, if we assume the SXR radiator was Ni, the required rotation velocity needed to be about a factor of 2 higher. Thus, we assume that all of the SXR signal originates from W, which allows for the calculation of the localW-concentrations using an ionization equilibrium neglecting transport. The latter assumption has been proven to be reasonable for W(e.g. [14]). From the W-concentration the total, local radiated power densities

due to W are derived using its cooling factor [1]. These power densities are presented in Fig.5(c) and (d). Please note that the radiation ring at the edge of the evaluation region might be an artefact yielded by larger uncertainties of the evaluation at plasma radii where the SXR-emissions are close to the Bremsstrahlungs-level. The 2D structure of the emissions inside of that ring are real and make apparent, why the spectrometer measurements underestimate the W-content of the core plasma. The measurement location of the spectrometer is indicated by white bars in Fig.5 and do not radially or poloidally coincide with the regions exhibiting the strongestW-emissions. The strong localized peaking itself is no big surprise, as this is very characteristic for so-called impurity accumulation. We note that the term impurity accumulation is used ambiguously and that in the present work we always refer to core localized impurity accumulation. In [15,16] it has been found that impurity accumulation occurs when turbulent transport in the plasma core is weak, and the collisional transport becomes more important. The cleaning effect of large turbulent core transport is not only based on diffusive effects, but also supported by a turbulent outward pinch for the impurities. Both turbulent effects require steep temperature gradients [17,16,18]. When the temperature gradients are weak neoclassical transport becomes important. If a gradient in the deuterium density exists, the neoclassical inward pinch arises for the impurities.

In Pulse No: 81913, the occurrence of impurity accumulation is consistent with the development of density peaking. In order to judge on the power fluxes inside the plasma a closer look into the radiation/heating balance of the core plasma of Pulse No: 81913 is necessary. Considerable radiative cooling is able to decrease the core T_e and will flatten the gradients in T_e, which causes a decrease of turbulent transport (e.g. [19]) and starts a feedback loop of transport and radiation. Thus, the SXR analysis is applied to the full time sequence using 25ms and 200ms time intervals in which the signals are averaged. The obtained 2D radiation profiles similar to those in Fig.5(c) and (d) are used to derive the total radiated power due toWin the core plasma. In Fig.6 the evolution of relevant core parameters are depicted. While the density peaking (cf. Fig.6 (a)) develops gradually and becomes maximal already at about 10.5s, the radiation peaking is almost constant up to about 10.0s and then starts rising until the end of the heating phase. The density peaking reaches values of 1.5 (i.e. the ratio of core ($r_{norm} = 0$) and pedestal-top densities) and the radiation peaking (derived from comparing two bolometer lines of sight) rises to values of 4 and keeps rising after 11.5s. It should be noted that the radiation peaking is very localized in the core as the peaking happens within about $r_{norm} = 0.4$. The W-radiation in the core (cf. Fig.6(b)) is at negligible levels at 9.0s and starts rising at about 9.75s consistently with the diagnosed radiation peaking. When comparing the NBI heating power within rnorm < 0.4 to the radiated power attributed to W via the SXR camera analysis, they become comparable only after 10.0s. The reason for the change in transport might be localized even more centrally. At the plasma volume within rnorm < 0.15, the radiation power density is strongly modulated by sawteeth already at 9.5s. At the end of the sawtooth cycle the radiation density is about a third of the heating power density - thus an impact on the Te-profiles and turbulence seems possible. This evolution is consistent with the general observation that impurity accumulation

starts in the plasma core, where gradients approach zero close to the magnetic axis. Clearly, this observation suggests that central impurity accumulation may be avoided by more localized core heating or a smaller level of W-concentration [20]. Both mechanisms have been reported before at ASDEX Upgrade [17,16,20] or JET [18]. ICRF heating at JET provides core localized heating and thus is a good candidate for controlling the impurity accumulation. This has been demonstrated in earlier campaigns (e.g. [18]), and the present work suggests that is also works for controlling W-accumulation.

4. SCREENING OF W

The erosion of W is localized in the divertor, where the ion flux is largest and during ELMs a considerable fraction of the W-erosion occurs [5,6]. For the inter-ELM phase the electron temperature has been found to be a controlling factor of the erosion process in the divertor, while impurities are always the sputtering species [5,6]. The erosion is quantified by spectroscopic measurements on lines of sight observing the W-surfaces. The Wflux is deduced from the photon fluxes using the S/XB-method [21]. The ratio of the total W-content and total W-flux gives the effective W-confinement time W. It is a figure of merit, which allows to quantify the efficiency of an eroded atom to enter the plasma bulk. Thus, τ_W integrates the prompt deposition, the screening mechanisms in divertor and scrape-off layer, pedestal transport and partly core transport in a single number. In [22,23] the edge transport and erosion has been modeled, and edge-localized modes (ELMs) have been identified to play a major role for control of impurities. More frequent ELMs have been observed to provide cleaner main plasmas, as impurities are flushed by the ELMs, while in between the ELMs they experience an inward pinch at the pedestal. In the present work deuterium gas puffing is used to increase the ELM frequency of discharges with low and high triangularity (low δ and high δ) shapes. In Fig.7(a) τ_W versus the ELM-frequency is depicted for 2.0MA plasmas performed at 2.2T. The data points exhibit a considerable scatter, but the expected trend of higher W at lower ELM-frequency is visible. No clear separation between the low and high triangularity is observed, which could be related to the scatter. In Fig.7(b) τ_W versus the deuterium gas rate is presented. For lower gas puff τ_W is systematically higher. In Fig.7(c) a clear relation between W and the energy confinement time τ_E becomes apparent. Note that the zero on the E-axis is suppressed. The W-screening is strongly enhanced for a moderate confinement degradation. Looking in more detail, the lower confinement either correlates to higher ELM-frequencies or higher deuterium gas puff levels. It should be noted that W only provides information about the screening of τ_W, however, the W-concentration is determined also by the source of W. The latter is a complicated function of power transported to the divertor, particle fluxes and impurity densities. For our limited data set the W-source is small for high gas puff rates and high ELM frequencies.

These findings support the strategy to operate at a non-zero gas puff level and an elevated ELMfrequency (e.g. ELM-pacemaking), while the slightly reduced confinement of the plasma [24] may be enhanced by additional means. This might be nitrogen seeding [25] or the exploitation of

an enhanced confinement due to a favorable -dependence [26]. The latter is observed for discharges at finite gas puffing levels when the highest beam heating powers are applied.

5. SUMMARY

The impact of tungsten eroded in the divertor on stability and confinement of plasma discharges is studied in JET featuring the ITER-like wall. A localized quantification of W has been developed by a combination of measurements from soft X-ray cameras and a VUV spectrometer. The soft X-ray cameras allow for a detailed accounting of core radiation and poloidal asymmetries. The latter are explained by parallel transport in the presence of centrifugal forces using rotation velocities consistent with charge-exchange recombination spectroscopy. Beam heated discharges are observed to develop central impurity accumulation for cases in which the central power balance is considerably influenced by W-radiation. In Pulse No: 81913, which is representative for most of the impurity accumulation cases, it could be shown that the impurity accumulation starts by radiation peaking in the very core, locally flattening the Te-profiles which in turn provides less turbulent transport and giving more weight to the neoclassical inward pinch. The importance of the radiation/ heating balance directly implies that the stability against impurity accumulation can be improved by more core localized heating or by a lower τ_W-impurity level. A study of theWconfinement time (τ_W) is presented in order to identify the parameters that allow to operate at low τ_W levels. τ_W is found to be a factor 100-500 smaller than the energy confinement time indicating the efficient screening by the divertor. At low levels of deuterium gas puff, which coincides with low ELM frequencies, W are systematically higher. At the same time strong density peaking is observed at low gas puff levels consistently with the collisionallity scaling of density peaking [26]. All the described effects sum up and provide an unfavorable situation at zero gas puff. Thus, a recommendation of the present work is to operate with minimum gas puff levels of about $1\text{-}2\times10^{22}$ electrons/s and use additional core heating means like ion cyclotron heating in order to maintain a stable core balance between heating and radiation.

ACKNOWLEDGEMENT

This work was supported by EURATOM and carried out within the framework of the European Fusion Development Agreement. The views and opinions expressed herein do not necessarily reflect those of the European Commission.

REFERENCES

[1]. Pütterich T. et al., Nuclear Fusion **50** (2010) 025012 (9pp).
[2]. Neu, R. et al., Physica Scripta **T138** (2009) 014038 (6pp).
[3]. Mathews, G.F. et al., Journal of Nuclear Materials (2012), submitted.
[4]. Brezinsek, S. et al., Journal of Nuclear Materials (2012), submitted.
[5]. Van Rooij, G.J. et al., Journal of Nuclear Materials (2012), submitted.
[6]. Dux, R. et al., Journal of Nuclear Materials **390-391** (2009) 858.

[7]. Geuer, A. et al., Plasma Physics and Controlled Fusion **44** (2002) 2091.
[8]. Thoma, A. et al., Plasma Physics and Controlled Fusion **39** (1997) 1487.
[9]. Pütterich, T. et al., Plasma Physics and Controlled Fusion **50** (2008) 085016.
[10]. Neu, R. et al., Importance of Tungsten Spectroscopy to the Success of ITER, CRC Press, Boca Raton, FL, USA, 2011.
[11]. Anton, M. et al., Review of Scientific Instruments **66** (1995) 3762.
[12]. Wesson, J. A., Nuclear Fusion **37** (1997) 577.
[13]. Czarnecka, A. et al., Plasma Physics and Controlled Fusion **53** (2011) 035009.
[14]. Asmussen, K. et al., Nuclear Fusion **38** (1998) 967.
[15]. Dux, R. et al., Journal of Nuclear Materials **313–316** (2003) 1150.
[16]. Dux, R. et al., Plasma Physics and Controlled Fusion **45** (2003) 1815.
[17]. Sertoli, M. et al., Plasma Physics and Controlled Fusion **53** (2011) 035024.
[18]. Puiatti, M. et al., Physics of Plasmas **13** (2006).
[19]. Ryter, F. et al., Nuclear Fusion **43** (2003) 1396.
[20]. Neu, R. et al., Nuclear Fusion **45** (2005) 209.
[21]. Coenen, J.W. et al., EPS Stockholm (2012), P1.036.
[22]. Pütterich, T. et al., Journal of Nuclear Materials **415** (2011) S334.
[23]. Dux, R. et al., Nuclear Fusion **51** (2011) 053002.
[24]. Joffrin, E. et al., 2012, this conference.
[25]. Giroud, C. et al., 2012, this conference.
[26]. Beurskens, M.N.A. et al., 2012, this conference.

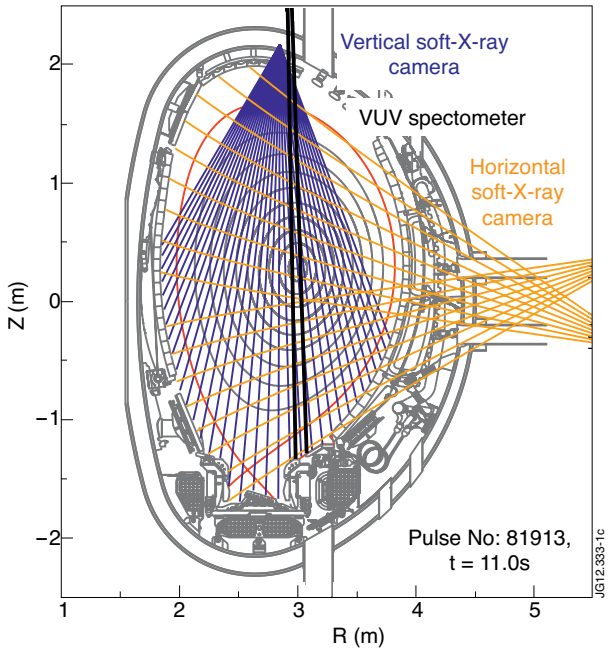

Figure 1: Diagnostic setup for determining the W-concentration and its poloidal asymmetry. The sight lines of soft X-ray cameras (blue and orange) and of a spectrometer (black) are featured together with the magnetic equilibrium of Pulse No: 81913 at 11.0s.

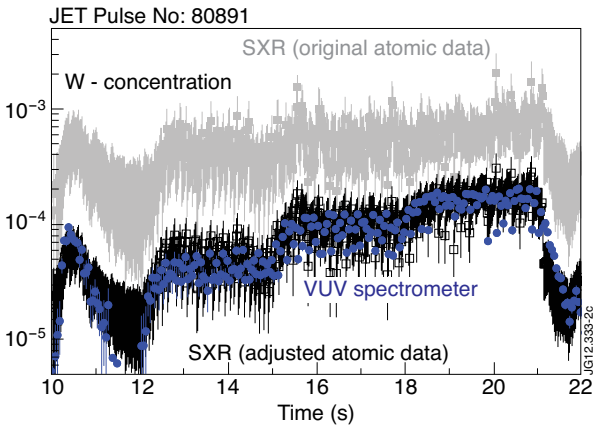

Figure 2: Comparison of the W-concentration measurements derived from the spectrometer measurements (blue) and the soft X-ray cameras (grey, black). The evaluation of the grey data uses the original atomic data, while the black data makes use of the presented adjustments.

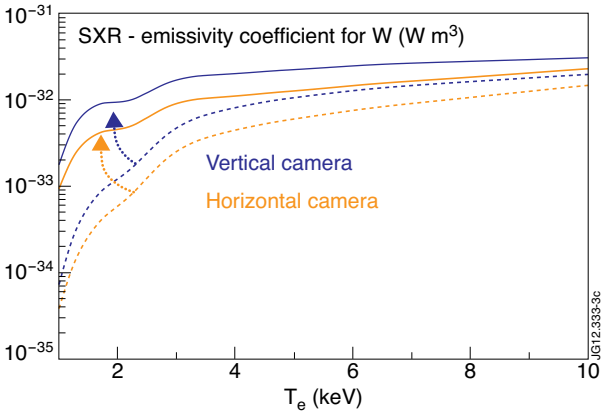

Figure 3: The soft X-ray emissivity coefficients for W derived for the vertical and horizontal SXRcameras. The data entering the analysis (solid lines) contain adjustments to the original data (dashed lines).

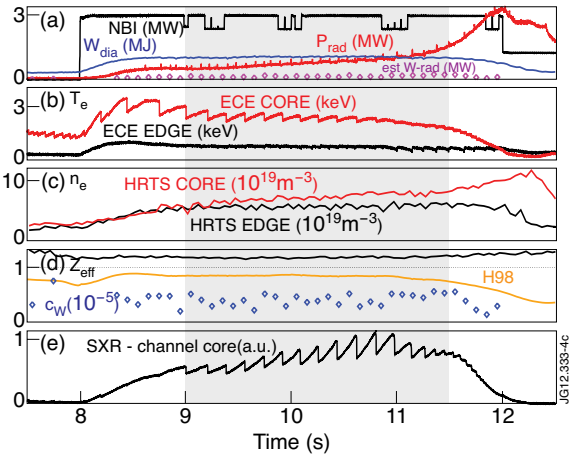

Figure 4: Time traces of selected parameters for Pulse No: 81913. Further information is in the text.

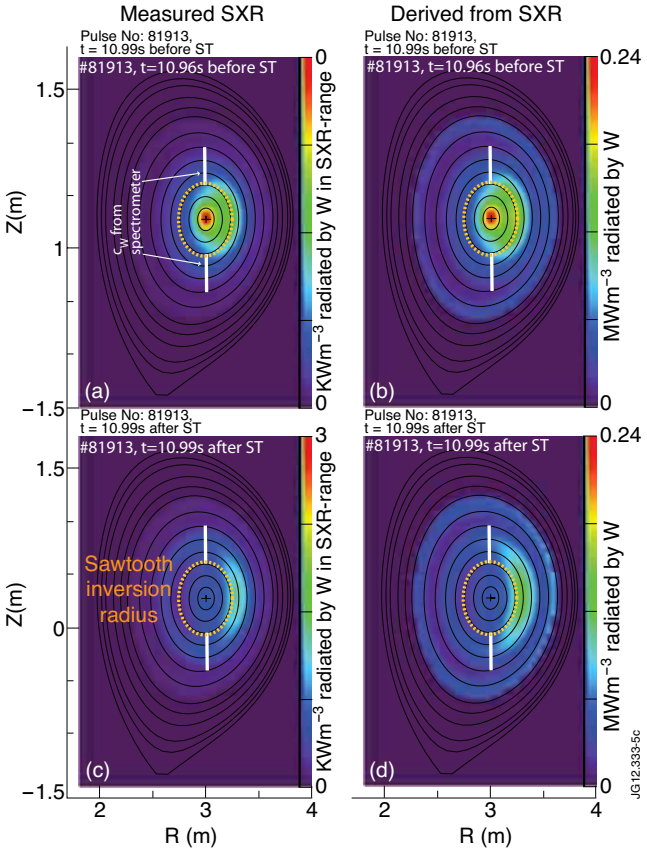

Figure 5: (a)+(b): 2D deconvolutions of the SXR signals before (a) and after (b) a sawtooth (ST). Bremsstrahlung contributions of low-Z elements have been subtracted. The white lines indicate the region of the W-concentration measurement based on the VUV spectrometer; (c)+(d): calculated total radiated power densities using the W-densities derived from (a) and (b).

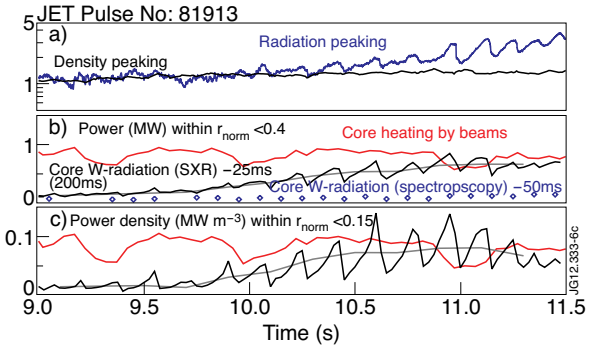

Figure 6: (a) time traces for density (black) and radiation (red) peaking; (b) heating and radiation power within rnorm < 0.4; (c) heating and radiation power densities within rnorm < 0.15.

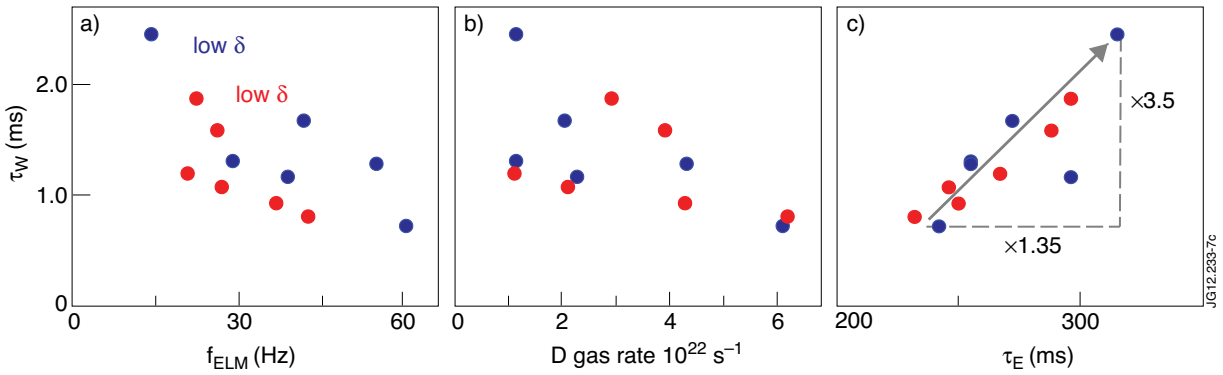

Figure 7: (a) W-confinement time (W) versus ELM-frequency (f_{ELM}) (b) τ_W versus deuterium gas rate (c) τ_W versus energy confinement time τ_E, factors of 3.5 in τ_W and 1.35 in τ_E are indicated; note the suppressed zero.